Concurrent Adaptation of Human and Machine Improves Simultaneous and Proportional Myoelectric Control

Janne M. Hahne*[1,2], Sven Dähne[1,3], Han-Jeong Hwang[1], Klaus-Robert. Müller*[1,3,4], Lucas C. Parra*[5]

[1]*Machine Learning Laboratory, Berlin Institute of Technology, D-10587 Berlin Germany*
[2]*Department of Neurorehabilitation Engineering, University Medical Center Göttingen Georg-August University Göttingen, D-37075, Germany*
[3]*Bernstein Center for Computational Neuroscience (BCCN), D-10587 Berlin, Germany*
[4]*Department of Brain and Cognitive Engineering, Korea University, Anam-dong, Seongbuk-gu, Seoul 136-713, Korea*
[5]*Department of Biomedical Engineering, City College of New York, New York, NY 10031 USA*

Abstract

Myoelectric control of a prosthetic hand with more than one degree of freedom (DoF) is challenging, and clinically available techniques require a sequential actuation of the DoFs. Simultaneous and proportional control of multiple DoFs is possible with regression-based approaches allowing for fluent and natural movements. Conventionally, the regressor is calibrated in an open-loop with training based on recorded data and the performance is evaluated subsequently. For individuals with amputation or congenital limb-deficiency who need to (re)learn how to generate suitable muscle contractions, this open-loop process may not be effective. We present a closed-loop real-time learning scheme in which both the user and the machine learn simultaneously to follow a common target. Experiments with ten able-bodied individuals show that this co-adaptive closed-loop learning strategy leads to significant performance improvements compared to a conventional open-loop training paradigm. Importantly, co-adaptive learning allowed two individuals with congenital deficiencies to perform simultaneous 2D proportional control at levels comparable to the able-bodied individuals, despite having to a learn completely new and unfamiliar mapping from muscle activity to movement trajectories. To our knowledge, this is the first study which investigates man-machine co-adaptation for regression-based myoelectric control. The proposed training strategy has the potential to improve myographic prosthetic control in clinically relevant settings.

1 Introduction

Electromyography (EMG) can be used to extract control signals for electrically powered hand prostheses from residual muscles. Currently available prostheses allow for control of a single degree of freedom (DoF) at any given time. To control two or more DoFs, mode switching between the DoFs, e.g. by a co-contraction, is needed for sequential actions. Significant progress has been made with classification-based approaches, which avoid the need for switching (for reviews see [1, 2, 3]). Since a classifier typically decides only which movement is activated, the control is limited to binary (on/off) sequential control at constant speed. Therefore the classification approach is often combined with a proportional estimator based on EMG amplitude that allows to modulate force or speed (also referred to as "mutex" [4]). The limitation of sequential control has been addressed by including additional classes with combined motion patterns ([5],[6]). However, as the speed of combined motions can be controlled in a fixed ratio only, there are still limitations. It is e.g. not possible to slowly rotate the hand while opening it quickly at the same time.

With regression-based techniques one can achieve a more flexible and fluid control of movement ([7, 8, 9, 10]). The essential difference with respect to classification is that a regressor does not select a pre-defined movement, but rather produces proportional outputs for all DoFs independently. Thus a regressor can be used to control several functions of a prosthesis simultaneously without the restrictions of a limited repertoire of movements. This allows for a smooth, natural and intuitive control which comes closer to the locomotion of an intact limb. A comparison of different regression techniques for myoelectric control is presented in [11]. With the appropriate selection of EMG features, simple linear models perform as well as more complex and computationally expensive methods such as artificial neuronal networks or kernel ridge regression. Real-time myoelectric control based on regression techniques is demonstrated in [12, 13, 14, 15, 16]. To train a regressor, typically motion or force labels are used, which for uni-lateral amputees can be measured at the intact limb during bilateral mirrored contractions [7]. Alternatively, one can use visual cues as movement targets ([14, 15, 16]), thus avoiding the need for cumbersome motion or force measurements that are not even possible in bilateral amputees.

Most studies that investigate regression-based control used contraction profiles with combined DoFs in the training protocol [7, 8, 13, 14, 15]. While combined movements are usually not difficult to execute for able-bodied individuals, they are challenging to acquire by individuals with amputation

or congenital limb deficiency as they do not have the intrinsic visual and proprioceptive feedback of the actual limb.

In this study we initially calibrate a regressor with individual movements and continue adaptation when performing combined movements allowing the man-machine interface to co-adapt ([17, 18]) to further improve real-time performance.

Several studies have investigated adaptation in myoelectric control. Most of them focused on the classification-based approach [19, 20, 21, 22] and employed adaptation with the goal to compensate for non-stationarities [23]. In classification, unsupervised adaptation is possible by using the classifier-output as adaptation target and considering only classifier decisions with high confidence. This can reduce the impact of slowly changing signal conditions, with the risk, however, that incorrect labels are used for adaptation leading to catastrophic failure [20]. In contrast, supervised adaptation that requires explicit user-interaction is more robust [19], though somewhat more cumbersome to use.

Powell et al. [24] demonstrated the great importance of user-training for classification-based myoelectric control. They used a strategy based on alternating open-loop calibration of the classifier and real-time evaluation using a virtual prosthesis. With the support of confusion matrices and measures for quantifying inter-class distances and within-class-consistencies, problematic movements were identified manually and improved by a targeted user-training.

Pilarski et al. [25] explored the possibility to use actor-critic reinforcement learning for training and adaptation of a myoelectric controller using a single, binary reward signal. This promising approach requires only minimal user interaction, but their study was limited to a single subject with only two contraction patterns. Thus, it remains to be seen whether this strategy can also efficiently be used to control several DoFs with free activation ratios, as required for independent proportional control.

In the present work we exploit the instantaneous feedback of the close-loop system, which in combination with a real-time learning algorithm allows the user and the machine to co-adapt and correct errors on the fly. Due to the common goal the user and the machine are enabled to adapt to a consistent and stable control strategy.

This concept of simultaneous (or co-adaptive) learning has been proven to be effective also in the context of brain-computer-interfaces ([17, 18, 26, 27]). Such co-adaptive systems are influenced by the speed with which both learners, the human and the machine, are adapting [18]. While learning speed of the human is not known and may vary between subjects, the adap-

tation speed of the machine can be controlled via hyper-parameters of the algorithm. To the best of our knowledge this is the first study that investigates real-time learning for regression-based myoelectric control.

2 Methods

2.1 Signal Processing Chain

2.1.1 Data Acquisition

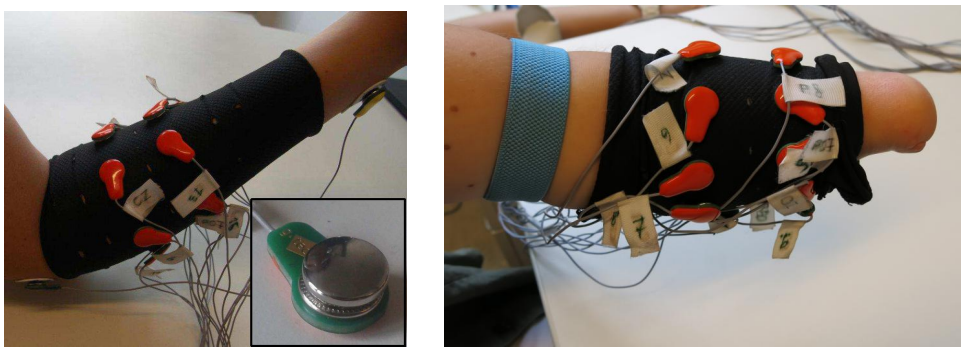

(a) (b)

Figure 1 – (a) EMG acquisition setup including the textile hose with integrated dry EMG electrodes mounted on able-bodied subject and custom-made dry EMG electrode mounted on pre-amplifier. (b) Setup mounted on a subject with congenital limb deficiency

The experimental setup comprised a 24 bit, 16 channel biosignal amplifier with an extension for dry electrodes (g.tec USBamp + g.tec Sahara), 16 custom-made dry, monopolar steel electrodes with 12 mm diameter that were integrated into a custom made stretchable textile hose (Fig. 1). The signals were sampled at 1200 Hz and frequencies above the Nyquist criterion were removed with internal low pass filters provided by the amplifier. All further processing and visualization were performed in MATLAB 12a 64 bit running on a 2.67 Ghz, dual-core personal computer with 8 GB RAM. An overview on the signal processing chain is given in Fig. 2.

The electrodes were equally distributed on two circles with a distance of 35 mm to each other and the circumference of the textile hose adapted to the forearm of the subject. For the able-bodied subjects the hose was placed on the dominant forearms and for the subjects with congenital limb deficiency

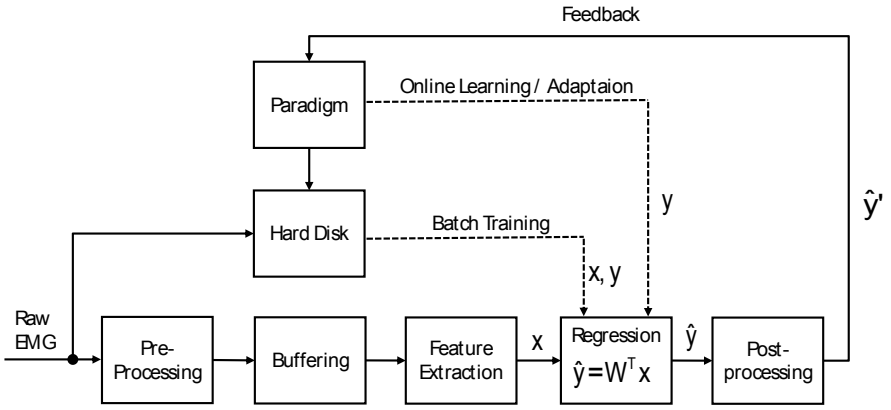

Figure 2 – Schematic overview of the signal processing chain. Pre-processing and feature extraction blocks are omitted in the batch training path for better readability.

on the affected side. For all subjects the electrodes were located approximately above the region with the largest diameter. Ground and reference electrodes were placed on bony sections of the wrist and the Olecranon with little EMG activity. We recruited ten able-bodied subjects (five females, five males, age 21-53) and two individuals with congenital limb-deficiency (congenital 1: female, age 36, residual limb length approximately 1/3 of the normal forearm; congenital 2: male, age 41, residual limb until wrist-level) to participate in this study. All experiments were in accordance with the declaration of Helsinki and were approved by the local ethics committee.

2.1.2 Pre-processing and Feature Extraction

The data were acquired and processed in blocks of 40 ms, corresponding to the update rate of the system ($f_{update} = 25\ Hz$) including the visual feedback. Sample-wise common-mean subtraction was performed to remove correlated noise and distortion that may be introduced by activity at the reference electrode and 50 Hz comb filters were applied to remove power-line interferences, including its harmonics. To reduce movement artifacts and maximize the signal-to-noise-ratio, the data were further filtered by 4th order Butterworth band-pass filters with a pass-band between 30 and 300 Hz. After pre-processing, the data were transferred into a queue buffer so that the last 12 s of data were available for feature extraction and real-time visualization.

We have shown in an offline-study that the log-variance of the band-pass filtered EMG is approximately linearly related to the joint angle and

thus allows for using computationally efficient linear regression techniques [11]. Therefore this feature was extracted for each channel, resulting in a 16-dimensional feature-vector $\mathbf{x}(t)$. The feature extraction was based on blocks of 200 ms with an increment of 40 ms, equivalent to the update rate of the system. This window duration is within the acceptable time delay between user command and prosthesis reaction [28],[29].

2.1.3 Regression and Post Processing

We applied an instantaneous, linear regression model where estimated outputs $\hat{\mathbf{y}}(t)$ (the position of a cursor on at 2D display) are obtained for each time instance t as a linear combination of the EMG features $\mathbf{x}(t)$:

$$\widehat{\mathbf{y}}(t) = \mathbf{W}^{\top}\mathbf{x}(t) \tag{1}$$

Each dimension in $\hat{\mathbf{y}}(t)$ corresponds to one DoF and $\mathbf{x}(t)$ is extended by the constant 1 to incorporate a bias compensation in $\mathbf{W}$. Thus, in our case the weight matrix $\mathbf{W}$ which characterizes the regression model is of size $< 17 \times 2 >$. The learning algorithm used to obtain $\mathbf{W}$ is described in section 2.2.

Since the instantaneous regression output $\hat{\mathbf{y}}(t)$ contains undesired high-frequency components caused by the stochastic nature of the EMG signal, an exponential moving-average filter (EMA) was applied to obtain a smooth controller output $\widehat{\mathbf{y}}\prime(t)$:

$$\widehat{\mathbf{y}}\prime(t) = \gamma\widehat{\mathbf{y}}\prime(t-1) + (1-\gamma)\widehat{\mathbf{y}}(t). \tag{2}$$

where the filter-constant γ controls the basic trade-off between smoothness of the movement trajectory and latency of the control. We set it to $\gamma = 24/25$, which subjectively provided a good compromise during execution. With these choices for temporal filtering, size of analysis window, and output smoothing the total delay of the system was less than 300 ms and subjects generally perceived an immediate system response.

2.2 Recursive Least Squares

Training a linear regression model with pre-recorded data can be done with a batch algorithm using the least mean-squares solution [30]:

$$\mathbf{W} = (\mathbf{X}\mathbf{X}^\top)^{-1}\mathbf{X}\mathbf{Y}^\top \tag{3}$$

In our supervised adaptation paradigm described below, the regression model is continuously updated every 40 ms during training. In cases like this, when new training samples are to be integrated continuously, on-line learning algorithms are more efficient than repeated batch training with increasing training sets. This saves memory, as there is no need to store the entire feature-set and is typically computationally less expensive [31]. We chose the exponential Recursive Least Squares (RLS) algorithm for this purpose [32]. This is a a powerful and stable extension of the batch algorithm. The RLS algorithm minimizes the following cost function:

$$\mathbf{E}(t) = \sum_{i=0}^{t} \lambda^{t-i} e^2(i) \tag{4}$$

where $e^2(i)$ is the squared error and $0 < \lambda \leq 1$ an exponential weighting constant which determines the influence of new data-samples and thus the speed and stability of adaptation. Based on an adaptive Wiener filter with this cost function the following set of update equations can be derived:

$$\begin{aligned}
\boldsymbol{\alpha}(t) &= \mathbf{y}(t)^\top - \mathbf{x}(t)^\top \mathbf{W}(t-1) && (5)\\
\mathbf{g}(t) &= \mathbf{P}(t-1)\mathbf{x}(t)\left(\lambda + \mathbf{x}(t)^\top \mathbf{P}(t-1)\mathbf{x}(t)\right)^{-1} && (6)\\
\mathbf{P}(t) &= \lambda^{-1}\mathbf{P}(t-1) - \mathbf{g}(t)\mathbf{x}(t)^\top \lambda^{-1}\mathbf{P}(t-1) && (7)\\
\mathbf{W}(t) &= \mathbf{W}(t-1) + \boldsymbol{\alpha}(t)\mathbf{g}(t) && (8)
\end{aligned}$$

$\boldsymbol{\alpha}(t)$ is the error with which the model from the previous update step would predict a new incoming data-sample at time instance t. $\mathbf{P}(t)$ is the inverse of the exponentially weighted sample covariance matrix and $\mathbf{g}(t)$ is the gain vector. Small values for λ cause a relatively fast adaptation and larger values (close to one) cause slower adaptation. For $\lambda = 1$ the algorithm becomes the *growing window RLS*, which gives equal weight to all samples and results in exactly the same solution as the batch algorithm with all collected data points. A detailed introduction on RLS is found in [32].

We initialize the model with the conventional batch algorithm ($\mathbf{W}(0)$ as Eq. (3) and $\mathbf{P}(0) = (\mathbf{X}\mathbf{X}^\top)^{-1}$) applied to the calibration data. This approach can be seen as a two-stage procedure: calibration with growing

window RLS followed by real time-adaptation with exponentially weighted RLS. We chose this scheme to give equal weight to all calibration samples and to start with the same condition for all learning constants to be investigated. In the experimental section we will investigate the influence of the adaptation speed, determined by the learning constant λ.

2.3 Experimental Paradigm

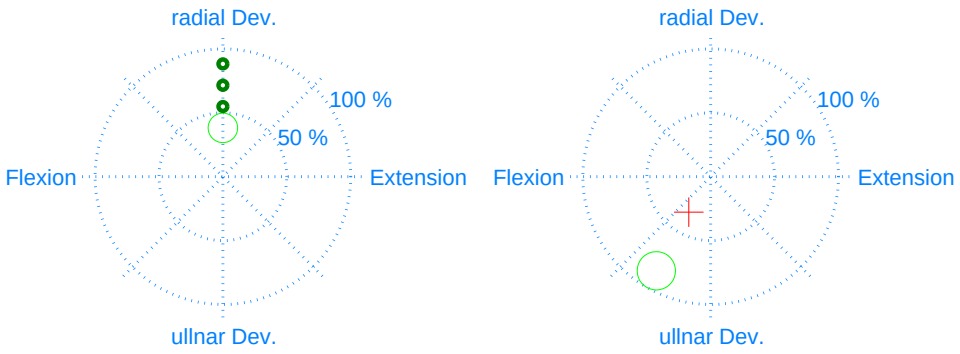

(a) (b)

Figure 3 – Experimental paradigm. (a) Display presented to the subject during calibration phase without feedback. The larger green "target-cursor" moves along pre-defined trajectories – the subject is asked to follow this cursor with wrist deflections. The upcoming target location is indicated with three small green circles to minimize delays between the instruction and user-reaction. (b) Display presented to the subject during performance evaluation and adaptation phases. The subject controls the red cross with muscle contractions and tries to hit the green circle, i.e. remain within the stationary target circle for one second without leaving it.

This study involved simultaneous movements of the two wrist DoFs flexion/extension and radial/ulnar deviation. The relative wrist angles were visualized on a user display by a two dimensional coordinate system in which the horizontal axis corresponds to flexion/extension and the vertical axis to radial/ulnar deviation (Fig. 3). The origin corresponds to the rest position of the wrist joint and the points on the unit circle to maximal wrist-inclinations. This control scheme is referred to as position-control and provides a direct view on the capabilities of the regressor [14].

2.3.1 Calibration Runs

In our previous offline-study [11] we found that even when trained with single DoF movements only, combined movements of the two DoFs investigated here can be estimated with relatively high accuracy by a linear regressor. For people with limb deficiency who are potential users of the proposed method it is very difficult to perform accurate combined movements without the intrinsic feedback of the limb. Including combined motions into open-loop calibration has almost no influence for able bodied subjects ([33]), while it can cause even negative effects in individuals with upper-limb deficiency who are often not able to reliably generate combined contractions with well-defined activation ratios. Therefore it was decided to compose the calibration runs for this study of single DoF activations only.

The subjects were instructed to follow visual targets that moved along predefined trajectories with their wrists angles and the subjects with congenital limb deficiency were asked to perform equivalent contractions. The trajectories were defined as follows: three seconds movement from rest position to maximal inclination, two seconds remaining in this position and three seconds returning to rest position. In each calibration-run this was repeated once for all four directions (Fig. 3 (a)). Interleaved with the trajectories also phases of "no-motion"-data were recorded (8 s per run) which were also included in the open-loop calibration.

2.3.2 Evaluation Runs

For closed-loop real-time evaluation, the current wrist position estimated from the EMG was visualized in real-time on a user screen by a red cursor (size 0.2 units). Circles with a radius of 0.15 units appeared within the coordinate system and the subject was asked to hit the stationary targets by moving the red cursor into the circle and remaining there for one second without leaving it. To allow for a fair and systematic comparison, the circle-positions were taken in randomized order from a pre-defined list that consisted of 8 equally spaced circles with a center-to-origin distance of 0.5 units and 16 circles at 0.85 units. The circle-positions are shown in Fig. 6. In order to approach each target from the rest-position and thus avoid possible influences of the randomized order (e.g. when two circles appear close to each other), before each regular target, an additional "zero-target" was placed at the origin of the coordinate system. Thus one evaluation run consisted of 24 regular targets and 24 zero-targets. The latter were not counted for the performance-evaluation. If a circle was not hit within ten seconds, a

time-out took effect and the run continued with the next target.

The metrics used to evaluate the performance (completion rate, completion time, overshoot ratio and path efficiency) are explained in table 1. We included all hit and missed targets in the performance metrics in order to avoid the potential bias caused by easier targets closer to the origin that were hit more frequently.

Table 1 – Performance Metrics

Metric	Description
Completion Rate	Ratio of successfully hit targets and total number of targets
Completion Time	Average time to hit a target, for missed targets the time-out is counted (10 s)
Overshoot Ratio	Number of times a target was left before 1 s dwell time, normalized by the total number of targets
Path Efficiency	Average ratio of shortest path to reach the target and actually traveled path-length

2.3.3 Adaptation Runs

For closed-loop real-time adaptation, the same paradigm as in the evaluation runs was applied. In order to adapt the model only for problematic regions, the adaptation started when a circle was not hit within the first five seconds after its appearance, and stopped when the target was hit or the ten second time-out occurred. The subjects were informed by an auditory signal about the start of the adaptation phase and were instructed to keep trying to hit the target. During the adaptation-phase the current feature vector was used to adapt the regression model (every 40ms) with the current target as reference. This evidently improved the regression model for the region of the current target. Since the target position is known to the algorithm during adaptation, a fair evaluation of the performance during these runs is not possible. Thus, data from the adaptation-phase was excluded for the performance evaluation.

2.3.4 Study Design

The goal of this study was to explore co-adaptive real-time learning as a tool to train regression algorithms for myoelectric control and to investigate the

influence of the adaptation speed within this two-learners problem consisting of human and machine. To compare the results of co-adaptive learning with those of conventional open-loop training and determine to which extend improvements may be caused by user adaptation alone, four control conditions were included, which will be explained below in more detail. A chronological overview of the experiment is provided in table 2. Between the runs the subjects were allowed to take breaks of arbitrary duration in which beverages and sweets were offered. An entire session lasted around 1 1/2 to 2 hours. None of the subjects reported muscular or mental fatigue.

In the beginning of the session the signal quality was checked by visual inspection of the filtered EMG during rest and contraction. The experimenter explained the paradigm to the subject and demonstrated the wrist movements, which were copied by the subject for training purpose. For the subjects with congenital limb-deficiency a real-time visualization of the EMG-amplitudes was used to verify that they generated different patterns for the four non-combined movements of the two DoFs used in this study. After one demonstration run to familiarize the subject with the paradigm, four calibration runs were recorded and used to generate a regression model using the conventional (open-loop) least-squares batch algorithm (Eq. 3). This model was tested with one evaluation run as a baseline condition denoted by "Init 1".

In the following phase, co-adaptive real-time learning was investigated. For each adaptation speed, two runs were performed: One adaptation run and one evaluation run. For each adaptation run the RLS algorithm was initialized as described in section 2.2 based on the first three calibration runs. This was done to utilize approximately the same amount of data for obtaining the adapted model as in the baseline condition. After completing each adaptation run, the adapted model was tested in one evaluation run. This was repeated for each learning speed λ. The values for λ to be tested (1.0, 0.995, 0.99, 0.98, 0.96) were selected empirically. To avoid confusing subjects, the values of lambda were gradually changed in increasing ordered for half of the subjects and in descending order for the other half.

To evaluate learning effects of the user, the same model as for the baseline condition was tested a second time after the user had gained more experience with the paradigm and the control ("Init 2"). Since the primary shortcoming of the baseline condition was a limited range of motion, we included a naive correction condition ("upscale") where the output was simply scaled by a user-specific factor that extended reach to the entire output space. The scaling factor was determined by analyzing the cursor-traces of runs 5 and 16 that were performed with the initial regression model. For the direction

with the shortest reach, the inverse of the maximal distance to the origin was used as factor, and in cases of inconsistency between the two runs the smaller factor was used. The factors applied in this study were in average 2.34 ± 0.38 (range: 1.82 to 2.94).

For a final control condition, four additional calibration runs were recorded in the end of the session and used to train a regression model as in the baseline condition. This was done in order to test if re-calibration after obtaining experience with the control could improve the performance in a final evaluation run ("re-calibration").

Table 2 – Chronological overview of the runs performed in this study

Run	Type	Init with run	Description
1 - 4	Cal		Calibration
5	Eval	1 - 4	Init 1
6,8,10,12,14	Adapt	1 - 3	Adaptation with different λ
7,9,11,13,15	Eval		Evaluation of adapted models
16	Eval	1 - 4	Init 2
17	Eval	1 - 4	Test upscaling
18 - 21	Cal		Re-calibration
22	Eval	18 - 21	Test Re-calibration

3 Results

We conducted experiments with ten able-bodied subjects and two individuals with congenital limb deficiency according to the experimental paradigm described in section 2.3. The closed-loop real-time performance was analyzed according to the quantitative metrics introduced in table 1 and qualitatively by direct inspection of the cursor trace and the location of hit and missed targets.

3.1 Quantitative Results

Real-time performance for all subjects was evaluated after co-adaptive learning with five different adaptation speeds and in four control conditions (Fig. 4 a-d). To test statistical differences between the conditions for the ten able-bodied subjects, one-way repeated-measure(RM)-ANOVA was conducted. All statistical analyses were done in SPSS and the significance threshold was set to 0.05. Since RM-ANOVA assumes equal variances for all condi-

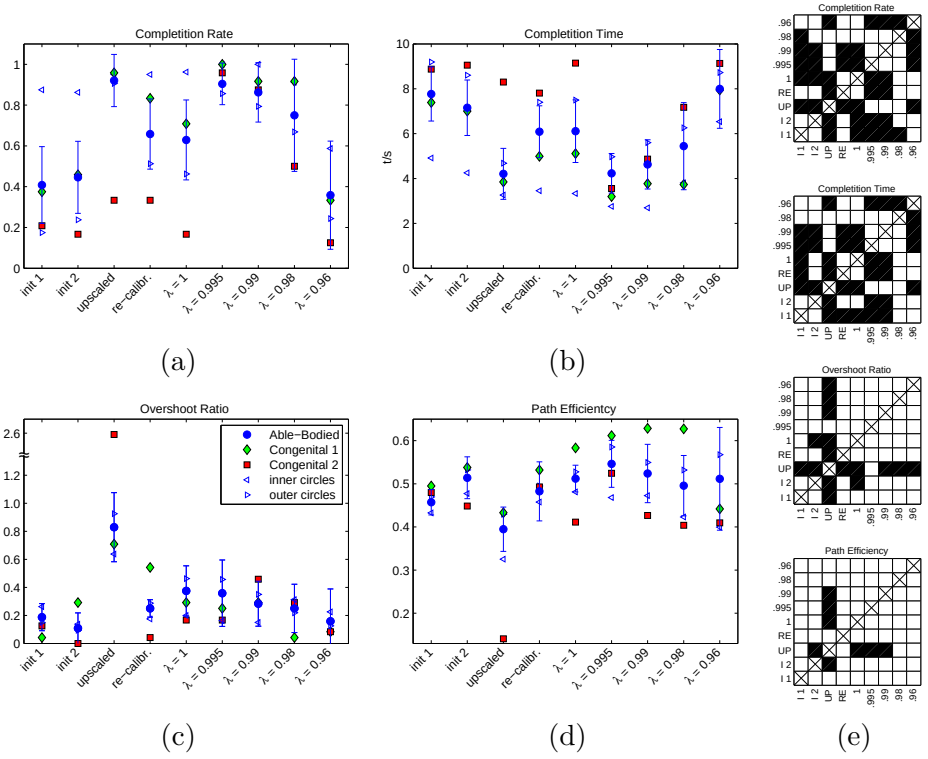

Figure 4 – Real-time evaluation results for the four control conditions and after adaptation with different λ. Blue circles and error bars show means and standard deviations across all able bodied subjects, the red squares and green diamonds indicate the performances of the two congenital subjects. The blue triangles show the mean performances for able-bodied subjects for targets with lower and higher distance to the origin separately. Panel (a)-(d) show completion rate, completion time, overshoot ratio and path efficiency. The plots in panel (e) show post-hoc pair-wise comparisons in which black fields indicate statistical significant differences between the corresponding conditions ($p < 0.05$). The best performance across all metrics is obtained after adaptation with $\lambda = 0.995$. Completion rate and time show similar results for the upscaled condition but the poor overshoot ratio and path efficiency obtained with the upscaled model indicate a significant drop in stability. The subjects with congenital limb deficiency show the same trends as able-bodied subjects and reach a similar performance after co-adaptive real-time learning.

tions, Mauchly's Test of Sphericity was conducted. A significant difference between the variances of each condition was found for *path efficiency*, therefore Greenhouse-Geisser correction [34] was done for this metric. For all four performance metrics, significant differences between conditions were found (completion rate: $F(8, 72) = 24.378$, $p < 0.001$; completion time: $F(8, 72) = 23.018$, $p < 0.001$; overshoot-ratio: $F(8, 72) = 13.625$, $p < 0.001$, path efficiency: $F(2.66, 23.98) = 4.664$, $p = 0.013$). A post-hoc paired t-test with Bonferroni correction for multiple comparisons was performed to identify the conditions with significant differences. Results of the statistical evaluation are provided in Fig. 4 (e).

Across the tests based on real-time learning, $\lambda = 0.995$ showed the best results with the highest completion rate, lowest completion time and highest path efficiency. The completion rate and completion time significantly improved compared to the baseline-condition "Init 1" while the overshoot ratio and path efficiency showed no significant difference.

Control condition "Init 2", which uses the same regression model as in condition "Init 1" showed a slight improvement in all metrics, but none of the differences between "Init 1" and "Init 2" were significant, suggesting limited benefit of user-adaptation alone. A similar trend was observed for the re-calibration condition. Here only completion time showed significant improvements. Despite performance improvements for "Init 2" and re-calibration, the performance of both models was still significantly lower than the closed-loop co-adaptive model (at $\lambda = 0.995$) in terms of completion rate and completion time, showing that co-adaptive real-time learning can further increase the overall performance of myoelectric control.

The upscaled model showed statistical significant improvements in the completion rate and completion time, similar to co-adaptive learning with suitable λ. However, the control became rather unstable. This is seen in the overshoot ratio which worsened significantly and showed the lowest performance among all conditions. The difference to the best co-adaptation condition is marginally significant ($p = 0.052$), and statistically significant relative to the other conditions. The upscaled condition showed also the lowest path efficiency which was significantly worse than for "init 2" and the model obtained from co-adaptive learning with suitable λ.

The individual results for targets with smaller and larger distance to the origin show that co-adaptive learning leads to the strongest improvements for the outer targets compared to the baseline conditions. However, even if the effects for the inner targets are weaker, for both types of targets the same trends are visible.

The two subjects with congenital limb deficiency showed similar trends

as the able-bodied subjects, except that "congenital 2" performed relatively poor in all control conditions. Especially the condition "upscaled" showed low performance in all metrics and the very high overshoot ratio and very low path efficiency indicate that the control was rather unstable. Remarkably, with co-adaptive learning both subjects with congenital limb deficiency performed as good as the able-bodied subjects. Moreover, the optimal learning constant was the same as for the able-bodied subjects ($\lambda = 0.995$).

3.2 Qualitative Results

Figure 6 shows cursor-traces and target hit maps for two representative able-bodied subjects and the two subjects with congenital limb deficiency. For the initial condition based on open-loop training ("I1") the range of motion indicated by the black traces is often limited such that targets located in the outer regions could not be reached. The accessible range remained almost unchanged in the second test with the same regression model after the subject gained more experience with the control ("I2"). Repeated open-loop training with new calibration runs recorded at the end of the session ("RE") improved range in some cases, but did not fully correct this deficiency.

In the evaluation runs after co-adaptive learning with $\lambda = 0.995$, the range improved for all subjects so that most targets could be hit or at least shortly entered. For a lower adaptation speed ($\lambda = 1$) the range increased only slightly. The fastest adaptation speed ($\lambda = 0.96$) led to a poor and often very asymmetrical range. This indicates that the regressor overfitted to the most recent adaptation targets and "forgot" the relation between EMG features and output-space for other regions. This was confirmed when inspecting the specific (random) order in which targets were presented.

Upscaling of the regression output ("UP") causes by definition an extended range of motion so that most targets could be reached. However, the controllability was much worse than in the tests after co-adaptive learning with suitable adaptation speed. While the straight traces after co-adaptive learning indicate that the subjects could approach the targets directly and with high confidence, the traces in the upscaled condition reveal that there were strong overshoots and that the subjects often had to correct the direction. In some cases (such as able-bodied 1 and congenital 2) the controllability was so poor that many targets that were clearly within the range of motion could be entered but not hit because the control was too unstable for reaching the 1 s dwell time before the 10 s time-out. The qualitative results for the individuals with congenital limb deficiency are comparable in all aspects to those of able-bodied individuals.

A direct investigation of the coefficients $\mathbf{W}$ during the adaptation process for the first DoF (flexion/extension) and the two subjects with congenital limb-deficiency is provided in figure 5. With increasing adaptation speed (smaller λ) the coefficients $\mathbf{w_1}$ are changing faster and start oscillating for too fast adaptation. For the best adaptation speed ($\lambda = 0.995$), the absolute values of some coefficients increased during the overall adaptation process while others decreased. Also the norm $\|\mathbf{w_1}\|$ did not necessarily increase as the case of "congenital 2" shows. This demonstrates that the improvements in the regression model achieved during adaptation do not simply correspond to an amplification of the output, but more specific adaptations occur.

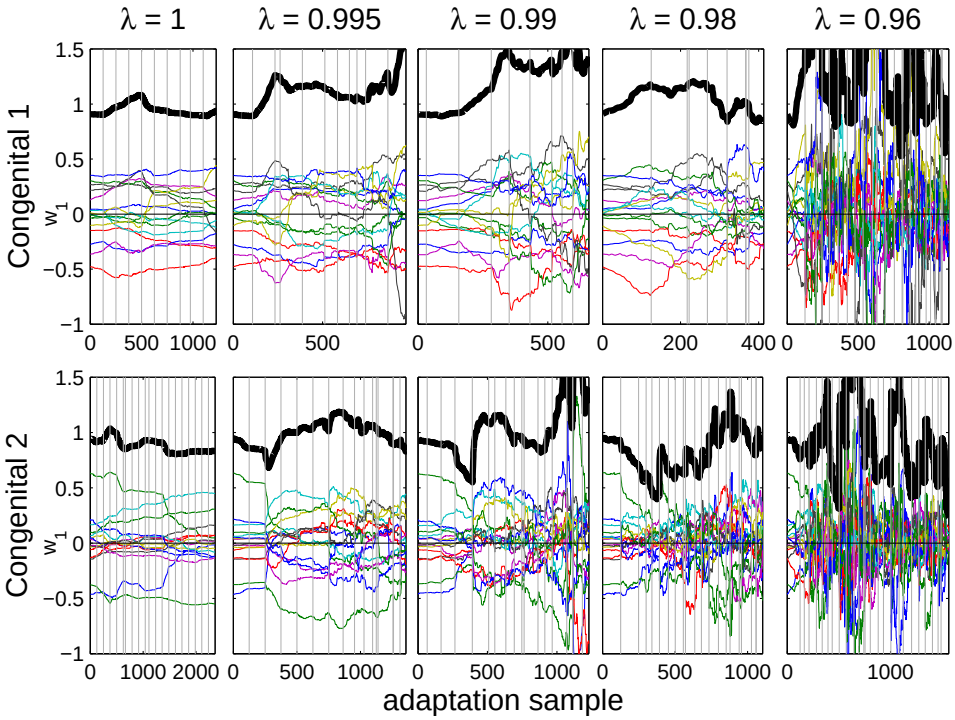

Figure 5 – Adaptation of $\mathbf{w_1}$ at different adaptation speeds for the two subjects with congenital limb deficiency. Each curve represents the development of one entry of $\mathbf{w_1}$ during the adaptation process, the bold black line the norm of $\mathbf{w_1}$ and vertical gray lines separate different adaptation targets. Similar results (not shown) were obtained for $\mathbf{w_2}$ and the able-bodied subjects.

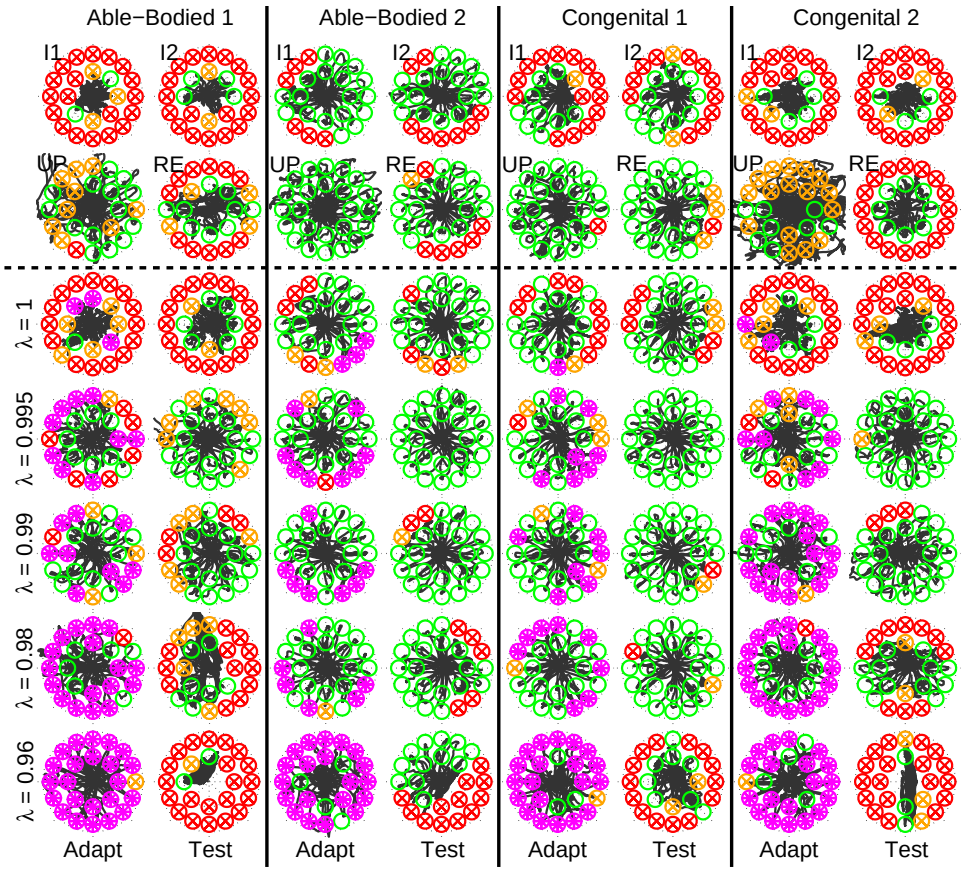

Figure 6 – Qualitative visualization of control performance for two able-bodied subjects with relatively low (able-bodied 1) and high (able-bodied 2) initial performance and for the two subjects with congenital limb deficiency. The black curves indicate the traces of the control cursor, green circles represent successfully hit targets, red circles missed targets and orange circles targets that were entered but not hit because of insufficient dwell time. For the adaptation runs green circles represent targets that were hit before adaptation started, violet circles targets that were hit during the adaptation phase and red circles targets that were missed despite adaptation. Above the dashed line the four control conditions are presented: Initial model tested in the beginning (I1) and towards the end of the session (I2), upscaled output (UP) and re-calibrated (RE). Below, the adaptation runs with different learning constants λ are shown (Adapt) and next to it, the test runs for the adapted models (Test). In the initial condition (I1) some parts of the outer regions were often not accessible and remained nearly unchanged in the 2nd test (I2). Re-calibration could only partly compensate for this limitation. Upscaling of the output led by definition to an extended range but made the control relatively unstable which led to many overshoots and made fine-control difficult. After adaptation with $\lambda = 0.995$, the range became more uniform and covered almost the entire range, while stability of the control was maintained.

4 Discussion

In this study we have shown that co-adaptive learning can significantly improve regression-based myoelectric control compared to open-loop calibration. We demonstrated that the benefits are not simply a result of user-adaptation or improvement in the training data as practice progresses. We conclude therefore that performance gains result from the interaction between the two concurrent learners. We also showed that simple corrective strategies based on off-line learning are inadequate. Importantly, co-adaptive learning allowed individuals with congenital deficiencies to perform simultaneous 2D proportional control at levels comparable to able-bodied individuals, despite having to learn a completely new and unfamiliar mapping from muscle activity to movement trajectories.

By providing a common target, co-adaptive learning permits the two learners — human and machine — to stably converge to a synergistic control strategy for independent proportional control of two DoFs. The conventional approach to myographic control leverages user-learning and machine-learning by interleaving phases of open-loop calibration and real-time user adaptation [24]. This can be relatively slow as the machine learns only once in each iteration, and the user does not receive feedback on improvements of the model until the next evaluation period. Thus, several iterations of this time-consuming process may be required until convergence is reached [24]. In our co-adaptive learning approach, both the algorithm and the user learn simultaneously in an interactive way. Due to the real-time feedback which is now provided during adaptation, the user is encouraged to continuously improve contraction patterns, which are immediately incorporated into the model.

A crucial trade-off in co-adaptive learning is that between stability and adaptation speed [18]. In the present system this trade-off is regulated by the learning constant of the recursive least-squares algorithm. We found that all subjects tested achieved best performance with a similar learning constant, suggesting that this parameter should be applicable to most individuals. Note that due to the two-stage procedure described in section 2.2, the number of calibration samples would influence the optimal value for λ. However, this can easily be compensated by normalizing the initialization of $\mathbf{P}$ by the ratio of calibration samples.

The case of "congenital 2" is of particular interest because this subject had poor performance in all control conditions. Those are the conditions that rely exclusively on open-loop calibration. Yet, closed-loop co-adaptive learning permitted this subject to identify muscle contraction pattern with

a performance that is on par with able-bodied individuals. This qualitative jump was not possible with user-learning because effective control requires not only that the user generates appropriate contractions, but for the machine to translate these into the correct 2D coordinates. Without the correct set of contractions the machine cannot learn, and without the correct mapping the user will not discover the correct muscle pattern. This chicken-and-egg problem is less severe for able-bodied individuals because they can rely on a known muscle contractions to independently control two DoFs. But regardless of the initial conditions, the co-adaptive learning allows the individual and machine to more readily identify a synergistic strategy within the allowed time.

The present work emphasized clinical feasibility. First, we selected a dry electrode system. While gel electrodes provide better signal quality, only dry electrodes are suitable for an application in prosthetics. Second, we used very efficient linear processing techniques that provide minimal latency and can be readily implemented in low-power and low-cost digital hardware required for clinical application [3]. Third, no measurements of kinematics or forces were needed and instead only visual cues were used for the initial calibration and adaptation. Aside from reducing the costs, this allows for applying the methods to a wide range of users, including bilateral amputees who stand to benefit the most from advanced hand prostheses. In this study we used 16 EMG-channels, as this allows for a non-targeted placement of the electrodes. A reduction of the number of channels is possible and can be done very efficiently with channel-selection techniques [35].

We have shown in previous offline-studies, which included motion-tracking based data labels that a linear regressor, calibrated with the individual DoFs flexion/extension and radial/ulnar deviation is able to estimate even combined movements with relatively high accuracy ([11, 33]). In this real-time study, combined movements could also be estimated after open-loop training the individual DoFs based on visual cues, but often some regions of the 2D output space were out of reach. Initial tests that involved also combined motions in open-loop training could not solve this issue. As it is so far not fully understood, how exactly the users transfer visual cues into kinematics and forces, inaccuracies in this transformation may be one of the factors that caused problems in open-loop calibration. This is particularly problematic in subjects with upper limb deficiency, who due to the missing feedback have difficulties in generating precise contraction patterns and where neither kinematics nor forces can be measured on the affected side.

Upscaling the output did not solve the problems of the open-loop trained model, as it led to a loss in fine-control. Even if this particular issue may be

partly reduced by heuristic compensation approaches, our co-adaptive learning approach provides a universal solution for a wider range of calibration problems. The essential advantage of the presented adaptation techniques is that the regression model is gradually improved while at the same time they leverage the human ability to learn and adapt to this changing machine control. This allows the user to more readily discover new contraction patterns that permit better simultaneous control for multiple degrees of freedom.

Future work will include co-adaptive learning for regression-based control of more than two DoFs. As the amount of possible combined movements grows exponentially with the number of DoFs, the strategy presented here is expected to be particularly useful. Our paradigm represents an efficient way to obtain new training examples only for regions that cannot be reached by a simple superposition of single DoF contractions. Initial tests with non-linear techniques such as kernel ridge regression did not exhibit significant improvements for the the current DoFs, but may be required for other DoFs (e.g. supination/pronation). Integrating them into our framework is straight-forward as efficient on-line learning algorithms are available also for non-linear regression techniques [16, 36]. Optimized spatial filters [37, 38], which enhance desired signal-properties in the raw-signal domain may also be beneficial when aiming to increase the number of DoFs.

Acknowledgment

This work was funded by DFG (MU 987/14-1) and the Marie Currie IAPP grant "AMYO", project number 251555 and by the National Research Foundation grant (No. 2012-005741) funded by the Korean government. We would like to thank Dario Farina for supporting this work.

References

[1] M. A. Oskoei and H. Hu, "Myoelectric control systems - a survey," *Biomedical Signal Processing and Control*, vol. 2, no. 4, pp. 275–294, Oct. 2007.

[2] E. Scheme and K. Englehart, "Electromyogram pattern recognition for control of powered upper-limb prostheses: state of the art and challenges for clinical use," *Journal of Rehabilitation Research and Development*, vol. 48, no. 6, pp. 643–659, Sep. 2011.

[3] N. Jiang, S. Dosen, K.-R. Muller, and D. Farina, "Myoelectric control of artificial limbs; is there a need to change focus?" *IEEE Signal Processing Magazine*, vol. 29, no. 5, pp. 152–150, Sep. 2012.

[4] A. Fougner, Ø. Stavdahl, P. Kyberd, Y. Losier, and P. Parker, "Control of upper limb prostheses: Terminology and proportional myoelectric control - a review," *IEEE Transactions on Neural Systems and Rehabilitation Engineering*, vol. 20, no. 5, pp. 663–677, Sep 2012.

[5] A. Young, L. Smith, E. Rouse, and L. Hargrove, "Classification of simultaneous movements using surface EMG pattern recognition," *IEEE Transactions on Bio-Medical Engineering*, vol. 60, no. 5, pp. 1250–1258, May 2013.

[6] M. Ortiz-Catalan, B. Hkansson, and R. Brnemark, "Real-time and simultaneous control of artificial limbs based on pattern recognition algorithms," *IEEE Transactions on Neural Systems and Rehabilitation Engineering*, vol. 22, no. 4, pp. 756–764, Jul. 2014.

[7] J. L. Nielsen, S. Holmgaard, N. Jiang, K. B. Englehart, D. Farina, and P. A. Parker, "Simultaneous and proportional force estimation for multifunction myoelectric prostheses using mirrored bilateral training," *IEEE Transactions on Biomedical Engineering*, vol. 58, no. 3, pp. 681–688, Mar. 2011.

[8] S. Muceli and D. Farina, "Simultaneous and proportional estimation of handkinematics from EMG during mirrored movements at multipledegrees-of-freedom," *IEEE Transactions on Neural Systems and Rehabilitation Engineering*, vol. 20, no. 3, pp. 371–378, May 2012.

[9] N. Jiang, J. L. Vest-Nielsen, S. Muceli, and D. Farina, "EMG-based simultaneous and proportional estimation of wrist/hand dynamics in uni-lateral trans-radial amputees," *Journal of NeuroEngineering and Rehabilitation*, vol. 9, no. 1, p. 42, Jun. 2012.

[10] E. Kamavuako, K. Englehart, W. Jensen, and D. Farina, "Simultaneous and proportional force estimation in multiple degrees of freedom from intramuscular EMG," *IEEE Transactions on Biomedical Engineering*, vol. 59, no. 7, pp. 1804–1807, May 2012.

[11] J. Hahne, F. Biessmann, N. Jiang, H. Rehbaum, F. Meinecke, K.-R. Müller, D. Farina, and L. Parra, "Linear and non-linear regression techniques for simultaneous and proportional myoelectric control,"

IEEE Transactions on Neural Systems and Rehabilitation Engineering, vol. 22, no. 2, pp. 269–279, Mar. 2014.

[12] N. Jiang, H. Rehbaum, I. Vujaklija, B. Graimann, and D. Farina, "Intuitive, online, simultaneous and proportional myoelectric control over two degrees of freedom in upper limb amputees," *IEEE Transactions on Neural Systems and Rehabilitation Engineering*, vol. 22, no. 3, pp. 501–510, May 2014.

[13] A. Ameri, E. Scheme, E. Kamavuako, K. Englehart, and P. Parker, "Real-time, simultaneous myoelectric control using force and position-based training paradigms," *IEEE Transactions on Biomedical Engineering*, vol. 61, no. 2, pp. 279–287, Feb. 2014.

[14] A. Ameri, E. N. Kamavuako, E. J. Scheme, K. B. Englehart, and P. A. Parker, "Real-time, simultaneous myoelectric control using visual target-based training paradigm," *Biomedical Signal Processing and Control*, vol. 13, pp. 8–14, Sep. 2014.

[15] A. Ameri, E. Kamavuako, E. Scheme, K. Englehart, and P. Parker, "Support vector regression for improved real-time, simultaneous myoelectric control," *IEEE Transactions on Neural Systems and Rehabilitation Engineering*, vol. Early Access Online, 2014.

[16] A. Gijsberts, R. Bohra, D. Sierra Gonzlez, A. Werner, M. Nowak, B. Caputo, M. A. Roa, and C. P. D. Castellini, "Stable myoelectric control of a hand prosthesis using non-linear incremental learning," *Frontiers in Neurorobotics*, vol. 8, p. 8, 2014.

[17] C. Vidaurre, C. Sannelli, K.-R. Müller, and B. Blankertz, "Machine-learning based co-adaptive calibration," *Neural computation*, vol. 23, no. 3, pp. 791–816, Feb 2011.

[18] C. Vidaurre, M. Kawanabe, P. von Bunau, B. Blankertz, and K.-R. Müller, "Toward unsupervised adaptation of lda for brain–computer interfaces," *Biomedical Engineering, IEEE Transactions on*, vol. 58, no. 3, pp. 587–597, Mar. 2011.

[19] J. W. Sensinger, B. A. Lock, and T. A. Kuiken, "Adaptive pattern recognition of myoelectric signals: exploration of conceptual framework and practical algorithms," *IEEE Transactions on Neural Systems and Rehabilitation Engineering*, vol. 17, no. 3, pp. 270–278, Jun. 2009.

[20] J. He, D. Zhang, and X. Zhu, "Adaptive pattern recognition of myoelectric signal towards practical multifunctional prosthesis control," in *Intelligent Robotics and Applications*, ser. Lecture Notes in Computer Science. Springer Berlin Heidelberg, Jan. 2012, no. 7506, pp. 518–525.

[21] H. Zhang, Y. Zhao, F. Yao, L. Xu, P. Shang, and G. Li, "An adaptation strategy of using LDA classifier for EMG pattern recognition," in *2013 35th Annual International Conference of the IEEE Engineering in Medicine and Biology Society (EMBC)*, Jul. 2013, pp. 4267–4270.

[22] X. Chen, D. Zhang, and X. Zhu, "Application of a self-enhancing classification method to electromyography pattern recognition for multifunctional prosthesis control," *Journal of NeuroEngineering and Rehabilitation*, vol. 10, no. 1, p. 44, May 2013.

[23] M. M.-C. Vidovic, L. P. Paredes, H.-J. Hwang, S. Amsüss, J. Pahl, J. M. Hahne, B. Graimann, D. Farina, and K.-R. Müller, "Covariate shift adaptation in EMG pattern recognition for prosthetic device control," in *EMBS 36th Annual International Conference of the IEEE*, 2014.

[24] M. Powell, R. Kaliki, and N. Thakor, "User training for pattern recognition-based myoelectric prostheses: Improving phantom limb movement consistency and distinguishability," *IEEE Transactions on Neural Systems and Rehabilitation Engineering*, vol. 22, no. 3, pp. 522–532, May 2014.

[25] P. Pilarski, M. Dawson, T. Degris, F. Fahimi, J. Carey, and R. Sutton, "Online human training of a myoelectric prosthesis controller via actor-critic reinforcement learning," in *2011 IEEE International Conference on Rehabilitation Robotics (ICORR)*, Jun. 2011.

[26] S. Lemm, B. Blankertz, T. Dickhaus, and K.-R. Müller, "Introduction to machine learning for brain imaging," *NeuroImage*, vol. 56, no. 2, pp. 387–399, May 2011.

[27] A. L. Orsborn, H. G. Moorman, S. A. Overduin, M. M. Shanechi, D. F. Dimitrov, and J. M. Carmena, "Closed-loop decoder adaptation shapes neural plasticity for skillful neuroprosthetic control," *Neuron*, vol. 82, no. 6, pp. 1380–1393, Jun. 2014.

[28] K. Englehart and B. Hudgins, "A robust, real-time control scheme for multifunction myoelectric control," *IEEE Transactions on Biomedical Engineering*, vol. 50, no. 7, pp. 848–854, Jul. 2003.

[29] T. R. Farrell and R. F. Weir, "The optimal controller delay for myoelectric prostheses," *IEEE Trans Neural Syst Rehabil Eng*, vol. 15, no. 1, pp. 111–118, Mar. 2007.

[30] C. M. Bishop, *Pattern Recognition and Machine Learning (Information Science and Statistics)*. New York: Springer, Oct 2007.

[31] L. Bottou, "Stochastic gradient descent tricks," in *Neural Networks: Tricks of the Trade*. Springer, 2012, pp. 421–436.

[32] M. H. Hayes, *Statistical digital signal processing and modeling*. New York: John Wiley & Sons, Apr. 1996, pp. 541–553.

[33] J. Hahne, S. Dähne, D. Farina, and K. Müller, "Separability of wrist motions in simultaneous and proportional myoelectric control," in *Bernstein Conference, Goettingen, DOI:10.12751/nncn.bc2014.0226*, Sep. 2014.

[34] S. W. Greenhouse and S. Geisser, "On methods in the analysis of profile data," *Psychometrika*, vol. 24, no. 2, pp. 95–112, 1959.

[35] H.-J. Hwang, J. M. Hahne, and K.-R. Müller, "Channel selection for simultaneous and proportional myoelectric prosthesis control of multiple degrees-of-freedom," *Journal of Neural Engineering*, vol. 11, no. 5, p. 056008, Oct. 2014.

[36] K.-R. Müller, S. Mika, G. Ratsch, K. Tsuda, and B. B. Schölkopf, "An introduction to kernel-based learning algorithms," *IEEE Transactions on Neural Networks*, vol. 12, no. 2, pp. 181–201, Jan 2001.

[37] J. Hahne, B. Graimann, and K.-R. Müller, "Spatial filtering for robust myoelectric control," *IEEE Transactions on Biomedical Engineering*, vol. 59, no. 5, pp. 1436 – 1443, May 2012.

[38] W. Samek, M. Kawanabe, and K.-R. Müller, "Divergence-based framework for common spatial patterns algorithms," *IEEE Reviews in Biomedical Engineering*, vol. 7, pp. 50–72, 2014. [Online]. Available: http://dx.doi.org/10.1109/RBME.2013.2290621